processes

MDPI

Article

Chemical Kinetic Mechanism and Experimental Validation of NOx Reburning–Equilibrium Disposal Technology

Shiqing Wang [1], Huadong Zhang [2,*], Xiaolong Qiu [3], Yutong Wang [1], Ping Xiao [3], Tao Luan [4] and Pengfei Li [5]

[1] State Key Laboratory of High-Efficiency Flexible Coal Power Generation and Carbon Capture Utilization and Storage, China Huaneng Group, Xiong'an 070001, China
[2] Huaneng Linyi Power Generation Co., Ltd., Linyi 273408, China
[3] Huaneng Clean Energy Research Institute, Beijing 102209, China
[4] School of Nuclear Science, Energy and Power Engineering, Shandong University, Jinan 250100, China
[5] State Key Laboratory of Coal Combustion, School of Energy and Power Engineering, Huazhong University of Science and Technology, Wuhan 430074, China
* Correspondence: zhanghuadong.chng@outlook.com

Abstract

To address the critical challenge of treating high-concentration nitrogen oxide (NOx) regeneration off-gas generated from Cold Oxidation Adsorption Process (COAP), an innovative concept termed 'NOx reburning–equilibrium disposal' is proposed. In this approach, concentrated NOx is re-injected into the boiler combustion zone, where it undergoes efficient ammonia-free decomposition under the high-temperature reducing atmosphere inherently present within the furnace. A comprehensive investigation was conducted through chemical kinetic simulations and laboratory-scale tubular furnace experiments. Chemical equilibrium calculations performed using CHEMKIN demonstrated that thermally generated NOx increases exponentially with temperature and that a distinct thermodynamic equilibrium concentration exists at each temperature. For example, the equilibrium NO concentration reaches 4781 mg·m^{-3} at 1500 °C. Within the temperature window of 1250–1450 °C, reducing atmospheres significantly enhanced NO reburning reduction efficiencies exceeded 70–90%, reaching up to 95% under strongly reducing conditions, substantially exceeding the less than 10% reduction achieved through purely thermal decomposition. Among the reducing species examined, CH_4 exhibited the strongest promoting effect by serving as an effective radical initiator. The simulation results were further verified through laboratory-scale tubular furnace experiments operating at temperatures up to 1700 °C. The combined theoretical and experimental findings systematically elucidate the reburning–equilibrium reaction mechanism of high-concentration NOx under high-temperature reducing conditions and establish a complete scientific evidence chain from fundamental theory to engineering validation. The proposed technology provides a novel pathway for deep ammonia-free NOx abatement in industrial flue gas treatment systems, such as those used in coal-fired power stations, gas-fired power stations, nuclear waste treatment facilities, glass furnaces and waste incineration plants.

Keywords: nitrogen oxides (NOx); reburning technology; chemical kinetic simulation; chemical equilibrium; ammonia-free denitrification

Check for updates

Academic Editor: Cherng-Yuan Lin

Received: 7 August 2026
Revised: 23 October 2026
Accepted: 29 October 2026
Published: 9 November 2026

Copyright: © 2026 by the authors. Licensee MDPI, Basel, Switzerland. This article is an open access article distributed under the terms and conditions of the Creative Commons Attribution (CC BY) license.

1. Introduction

The Nitrogen oxides (NOx) emitted from coal-fired combustion systems are key precursors to fine particulate matter ($PM_{2.5}$) and tropospheric ozone (O_3) [1,2]. Their deep

reduction has become an essential requirement for achieving China's "Dual Carbon" goals and strengthening air pollution control [3–5]. According to statistics released by the Ministry of Ecology and Environment of China, NOx emissions from major industrial sectors, including power generation, steel manufacturing, and cement production, account for more than 60% of the national total [6,7]. Through complex photochemical reactions, these emissions are transformed into secondary aerosols, which constitute a major source of regional haze and photochemical smog pollution [8]. With the implementation of policies such as the 14th Five-Year Comprehensive Work Plan for Energy Conservation and Emission Reduction and the Action Plan for Continuous Air Quality Improvement, NOx emission limits for industrial flue gases have become increasingly stringent [9,10]. In some regions, NOx emission concentrations are required to remain below 30 $mg \cdot m^{-3}$ at the reference oxygen content, indicating a transition from 'ultra-low emissions" toward "near-zero emissions' [11,12].

The mainstream technological route, represented by low-NOx combustion coupled with selective catalytic reduction (SCR), is capable of meeting current ultra-low emission standards [13]. However, several inherent limitations have become increasingly apparent under evolving operational conditions [14,15]. First, SCR catalysts typically exhibit optimal activity within a temperature range of 300–420 °C [16]. During deep load regulation and low-load operation of coal-fired units, flue-gas temperatures often fall below this window, resulting in a significant decline in denitrification performance [17]. This issue frequently coincides with periods of elevated NOx emission fluctuations during boiler start-up, shutdown, and load-changing operations. SCR systems require the continuous injection of ammonia or urea as reducing agents [18]. In practical operation, uneven mixing between ammonia and flue gas, as well as localized catalyst deactivation, is difficult to avoid [19]. Consequently, ammonia slip can occur, leading to secondary particulate formation [20]. Furthermore, escaped ammonia reacts with SO_3 in the flue gas to form ammonium bisulfate, which causes downstream equipment corrosion and blockage, thereby increasing operational and maintenance costs [21].

Vanadium–titanium-based SCR catalysts are continuously subjected to poisoning and fouling by alkali metals (K and Na), alkaline-earth metals (Ca), heavy metals (As and Pb), and fly ash [22]. Their service life is typically limited to 3–5 years. For a single 600 MW coal-fired unit, catalyst replacement costs may reach tens of millions of yuan, while disposal of spent catalysts introduces additional solid-waste management challenges [23]. Moreover, the extensive storage and transportation systems required for reducing agents represent potential safety hazards [24]. Therefore, there is an urgent need to develop a highly efficient NOx control technology that is free from secondary pollution, does not require external reducing agents, and can operate effectively over a wide load range, thereby supporting increasingly stringent emission standards [10,25,26]. Cold Oxidation Adsorption Process (COAP) has emerged as a promising alternative capable of integrated multi-pollutant removal. By employing solid adsorbents with tailored pore structures and surface chemistries, such as modified zeolites and metal–organic frameworks (MOFs), NOx can be selectively captured at relatively low temperatures (ambient temperature to approximately 150 °C) [1]. Simultaneously, acidic pollutants including SO_2 and HCl can also be removed. This technology offers both environmental and resource-utilization advantages while producing neither solid nor liquid wastes [27,28].

However, a common bottleneck impeding its industrial application arises during adsorbent regeneration [29,30]. After saturation, the adsorbent must be thermally regenerated, releasing a regeneration off-gas characterized by a very small flow rate (typically 1–3% of the original flue-gas volume) but an extremely high NOx concentration, often reaching tens of thousands of milligrams per cubic meter. For a representative COAP system treating 300,000 $m^3 \cdot h^{-1}$ of flue gas with an inlet NOx concentration of 200 $mg \cdot m^{-3}$ and

a removal efficiency of 95%, the regeneration off-gas may contain NOx concentrations as high as 10,000–20,000 mg·m^{-3}. Application of conventional SCR technology to such highly concentrated streams would result in excessive catalyst loading, dramatically increased reducing-agent consumption, oversized reactor volumes, and elevated risks of ammonia slip. Consequently, efficient, economical, and environmentally benign treatment of these concentrated NOx streams has become a critical challenge limiting the industrial deployment of COAP technology. Reburning technology, also referred to as fuel-staged combustion, is an effective approach for NOx reduction by introducing secondary fuels, such as natural gas, pulverized coal, or biomass, into high-temperature regions of the furnace to establish a locally reducing atmosphere [31]. The underlying chemical mechanism involves the thermal decomposition of secondary fuels under oxygen-deficient conditions, generating abundant hydrocarbon fragments and reactive radicals (e.g., CH_3, CH_2, and H), which subsequently react with NO and ultimately convert nitrogen species into harmless N_2 [32]. This technology requires no additional ammonia-based reducing agents, produces no secondary pollutants, and can be implemented through modifications to existing combustion facilities. Nevertheless, owing to limitations in secondary fuel supply and mixing uniformity, the NOx removal efficiency of conventional reburning systems is generally limited to 40–60%, making it difficult to independently satisfy ultra-low emission requirements.

To overcome the aforementioned challenges, this study proposes a novel concept termed 'NOx reburning–equilibrium disposal', in which the highly concentrated NOx regeneration off-gas produced by the COAP is treated as a special gaseous reburning medium and precisely injected into the primary combustion or burnout zones of a boiler. By utilizing the inherent high-temperature environment (>1200 °C) and strongly reducing atmosphere rich in CO, H_2, and CH_4, efficient ammonia-free decomposition of NOx can be achieved. The uniqueness of this concept lies in the principle of "waste treatment by waste utilization," whereby the most difficult waste stream generated during the COAP is transformed into a reactant within the reburning process and ultimately eliminated within the same combustion system. Successful implementation of this strategy would bridge the 'last mile' toward industrial deployment of COAP technology and establish a complete technological chain from deep flue-gas purification to environmentally benign treatment of concentrated regeneration exhaust.

Accordingly, the present study aims to systematically elucidate the reburning–equilibrium reaction mechanism of high-concentration NOx under high-temperature reducing conditions, clarify the coupling relationship and dominant mechanisms between thermal decomposition and reduction enhancement by reducing atmospheres, and comprehensively evaluate the engineering feasibility of this novel technological pathway.

- This work, to the best of our knowledge, systematically uses high-concentration NOx-containing regeneration off-gas as a reburning reagent for the first time.
- The NOx reduction is investigated under high-temperature gas-phase conditions of 1500–2000 °C.
- PSR kinetic simulations are combined with experiments.
- The concept of "waste treatment by waste utilization" is emphasized.

2. Materials and Methods

To systematically verify the feasibility of the proposed NOx reburning–equilibrium disposal technology, a progressive research framework integrating theoretical modeling and experimental validation was adopted. Chemical kinetic simulations were first performed to elucidate the underlying reaction mechanisms and determine key operational parameters, followed by laboratory-scale tubular furnace experiments for model verification. The detailed methodologies employed in both approaches are described below.

2.1. Construction of the Chemical Kinetic Model

2.1.1. Modeling Tools and Boundary Conditions

Chemical kinetic simulations were conducted using the CHEMKIN2022 software package. A Perfectly Stirred Reactor (PSR) model was employed as the core reactor configuration, assuming an ideal homogeneous reaction system with complete mixing and uniform temperature distribution. This assumption is consistent with the strong turbulence and rapid mixing characteristics typically observed in practical combustion zones.

Transient simulations were performed to track the temporal evolution of NO concentration. Based on the estimated residence time within industrial boiler combustion zones, the reaction duration was set to 3 s to ensure that the system approached a steady-state (equilibrium) condition. The investigated temperature range covered 500–2000 °C under atmospheric pressure (1 atm). The temperature inside the boiler furnace is generally above 1200 °C, and the flame-center temperature can reach above 1600 °C. On the basis of these conditions, the upper temperature limit for the numerical simulation was set to 2000 °C.

The chemical reaction mechanism adopted in this study was the extensively validated GRI-Mech 3.0 mechanism together with its nitrogen-species extensions. The mechanism comprises 53 chemical species and 325 elementary reactions, encompassing C_1–C_2 fuel oxidation pathways as well as thermal, prompt, and fuel-NOx formation and reduction submechanisms. It is particularly suitable for describing detailed NO reduction pathways under reducing conditions. Although GRI-Mech 3.0 was originally developed for natural gas combustion, its nitrogen chemistry models have been extensively validated and are suitable for simulating NOx formation and reduction in pulverized coal combustion. Regarding the potential release and transformation of char nitrogen (Char-N) during pulverized coal combustion, this work incorporated a heterogeneous reaction model for char into the GRI-Mech 3.0 model based on experimental conditions to ensure that the simulation aligns with the experimental conditions. Rate-of-production and sensitivity analyses were further employed to identify the key elementary reactions governing NO reduction.

A dual-inlet configuration was established to represent the oxygen-deficient combustion products from the primary combustion zone and the secondary injection stream containing highly concentrated NOx. The total injected NOx flow rate was fixed at 1/200 of the main flue-gas flow rate, with a correspondingly elevated inlet NO concentration.

In the NOx reburning system, the high-concentration NOx desorbed by heating in the adsorption-regeneration system (after SO_2 has been removed by the sodium metabisulfite system) is returned to the bottom-layer underfire air of the boiler burner and uniformly mixed into the air supply system. The injection location was selected at the bottom layer of the burner mainly for the following reasons: the bottom-layer underfire air has the longest travel distance to the combustion zone, which ensures that the returned NOx has sufficient residence time in the reducing atmosphere; the bottom-layer underfire air mixes fully with the pulverized-coal flow, which facilitates sufficient contact between the returned NOx and the reducing radicals generated by pulverized-coal combustion; and this location avoids disturbing the aerodynamic field of the main combustion zone, thereby ensuring combustion stability. The injection location of the high-concentration NOx is at the bottom layer of the boiler burner.

Based on different operating scenarios, six simulation models were developed:

Model I: Pure thermal NOx formation model;

Model II: Pure thermal decomposition model for recycled NOx in conventional furnaces;

Model III: Pure thermal decomposition model for recycled NOx in plasma furnaces;

Model IV: Thermal decomposition and reduction model for recycled NOx in plasma furnaces;

Model V: Thermal decomposition and reduction model for recycled NOx in pulverized-coal furnaces;

Model VI: Thermal decomposition and reduction model for recycled NOx in gas-fired furnaces.

The principal boundary conditions employed in the simulations are summarized as follows:

(1) The term "pure thermal conditions" refers exclusively to NO formation and decomposition induced by heating air. Only O_2 and N_2 were considered as the major air constituents, with molar fractions of 21% and 79%, respectively. Minor components, including inert gases, water vapor, and CO_2, were neglected because of their negligible influence on NO formation and decomposition.

(2) High-, medium-, and low-concentration NO conditions correspond to typical engineering scenarios encountered in plasma furnaces, pulverized-coal boilers, and gas-fired boilers, respectively. Specifically, high NO concentrations in plasma furnaces range from 2000 to 6000 mg·m^{-3}, medium concentrations in pulverized-coal boilers range from 200 to 1000 mg·m^{-3}, and low concentrations in gas-fired boilers range from 50 to 200 mg·m^{-3}. When the terms "high concentration" and "enrichment" are simultaneously used, they specifically denote concentrated regeneration off-gases with NO concentrations generally exceeding 10,000 mg·m^{-3} and, in some cases, surpassing 100,000 mg·m^{-3}.

(3) Based on measured data from typical boiler reburning zones, reducing atmospheres were classified into two categories according to their intensity. The strong reducing atmosphere consisted of 8.0% CO, 4.0% H_2, and 2.0% CH_4 on a molar basis, whereas the weak reducing atmosphere contained 3.0% CO, 2.0% H_2, and 0.5% CH_4.

2.1.2. Data Processing Methods

The simulation data were processed according to the following procedures:

(1) The simulation results indicated that several models shared similar boundary conditions and differed only in NOx concentration levels. Therefore, the results were consolidated into three groups for presentation and discussion. Group I corresponds to the pure thermal NOx formation model (Model I); Group II includes the pure thermal decomposition models for recycled NOx in conventional and plasma furnaces (Models II and III); and Group III comprises the thermal decomposition and reduction models for recycled NOx in plasma, pulverized-coal, and gas-fired furnaces (Models IV–VI).

(2) The NO reduction efficiency was calculated as follows:

$$\eta = \frac{\text{Cin} - \text{Cout}}{\text{Cin}} \times 100\%$$

where Cin and Cout denote the inlet and outlet NO concentrations, respectively.

(3) To satisfy the requirements of CHEMKIN calculations, all gas compositions in the simulations were specified on a molar basis (vol%). Considering that industrial applications conventionally express concentrations in mg·m^{-3}, all simulation results were converted accordingly when compared with engineering or experimental data.

(4) In the laboratory experiments, gas concentrations were initially recorded in mg·m^{-3} according to instrument readings and subsequently converted into molar concentrations during data processing to facilitate direct comparison with the simulation results.

2.2. Laboratory-Scale Tubular Furnace Experimental Platform

The schematic diagram of the COAP system is shown in Figure 1. To verify the accuracy of the theoretical model, a high-temperature tubular furnace experimental system was established, and the data obtained from this system were used to validate the simulation results of the theoretical model. The high-temperature tubular furnace experimental system mainly consists of a high-temperature tubular furnace, a gas supply unit, a steam generation unit, and a flue gas analysis unit. The high-temperature tubular furnace is heated by silicon carbide rods, has a maximum operating temperature of 1700 °C, an inner diameter of 50 mm, a constant-temperature zone length of 300 mm, and a temperature control accuracy of ±1 °C.

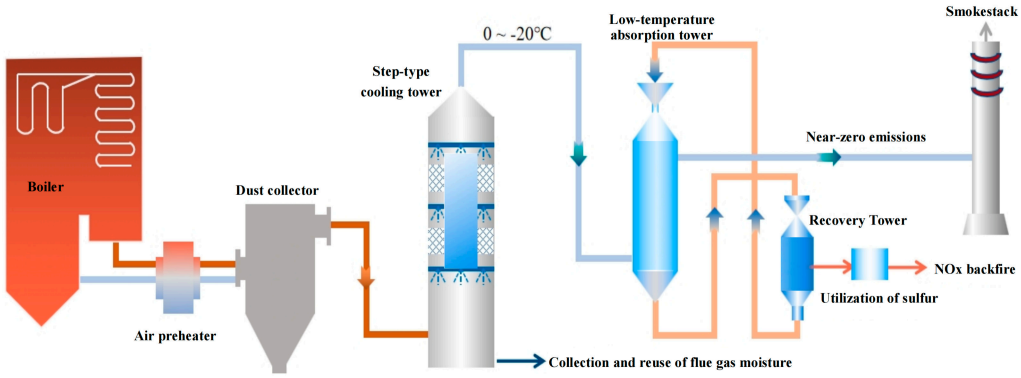


Figure 1. The schematic diagram of the COAP system.

The gas supply unit consists of high-pressure cylinders containing N_2, O_2, CO_2, NO, and CO. The flow rate of each component is precisely adjusted by mass flow controllers (MFCs), with a control accuracy of ±1% F.S. The total flow rate is controlled at 180 mL/min (standard conditions). The steam generation unit produces steam by N_2 bubbling with a heating mantle, and the steam concentration is controlled by adjusting the temperature of the heating mantle.

After mixing, the gas enters the high-temperature tubular furnace for reaction. The outlet gas is cooled and then enters the flue gas analyzer for continuous online detection. The flue gas analyzer uses a chemiluminescence method to detect NO/NO_x and electrochemical sensors to detect O_2 and CO, with a measurement accuracy of ±1%. All data are recorded in real time by a data acquisition system at a sampling frequency of 1 Hz.

The equipment used in this study is described as follows: the high-temperature tubular furnace is a GSL-1700X unit supplied by Hefei Kejing Materials Technology Co., Ltd. (Hefei, China); the portable gas detector is an MS400 unit supplied by Shenzhen Yiyuntian Electronics Co., Ltd. (Shenzhen, China) (measurement range 66,950 mg/m^3, measurement accuracy ±1 mg/m^3); the digital display electric heating mantle is a ZNHW unit supplied by Tianjin Gongxing Laboratory Instrument Co., Ltd. (Tianjin, China); and the high-purity nitrogen (99.999%), high-purity oxygen (99.999%), carbon dioxide (99.5%), NO standard gas (~80,000 mg/m^3), and CO standard gas (~3749 mg/m^3) were all supplied by Jinan Deyang Special Gas Co., Ltd. (Jinan, China).

3. Results and Discussion

To further elucidate the mechanisms governing NOx formation and reduction, the established chemical kinetic models were systematically validated through both theoretical simulations and laboratory experiments. CHEMKIN-based simulations were performed to investigate NOx formation and reduction behaviors under various operating conditions, with particular emphasis on extracting general principles applicable to engineering practice.

Subsequently, laboratory-scale tubular furnace experiments were conducted to verify the reliability of the theoretical predictions.

3.1. Simulation Results and Theoretical Analysis

Two representative high-temperature environments are commonly encountered in industrial systems. The first corresponds to high-temperature conditions with limited reducing species, such as plasma melting furnaces before feedstock introduction or conventional boilers operating under high excess-air coefficients. The second is characterized by both high temperatures and abundant reducing components, including plasma furnaces after material feeding and combustion zones retrofitted with low-NOx burners that create strongly reducing atmospheres. Accordingly, the present simulations focused on two aspects: (i) the pure thermal formation and decomposition behavior of NO under high-temperature, non-reducing conditions, and (ii) the reburning reduction characteristics of NO under high-temperature reducing atmospheres.

(1) Characteristics of Pure Thermal NOx Formation

The pure thermal NO formation model was employed to calculate thermal NO concentrations generated by heating air at different temperatures. The results are presented in Figure 2. The concentration of thermal NO increased continuously with increasing temperature. Below 1200 °C, the NO concentration remained essentially zero. A trace amount of NO (0.5 mg·m^{-3}) first appeared at 1300 °C, increased to approximately 120 mg·m^{-3} at 1500 °C, and subsequently accelerated, reaching 9248 mg·m^{-3} at 1800 °C. These results indicate that thermal NO formation is negligible below 1500 °C but becomes increasingly significant at higher temperatures, exhibiting an approximately exponential dependence on temperature.

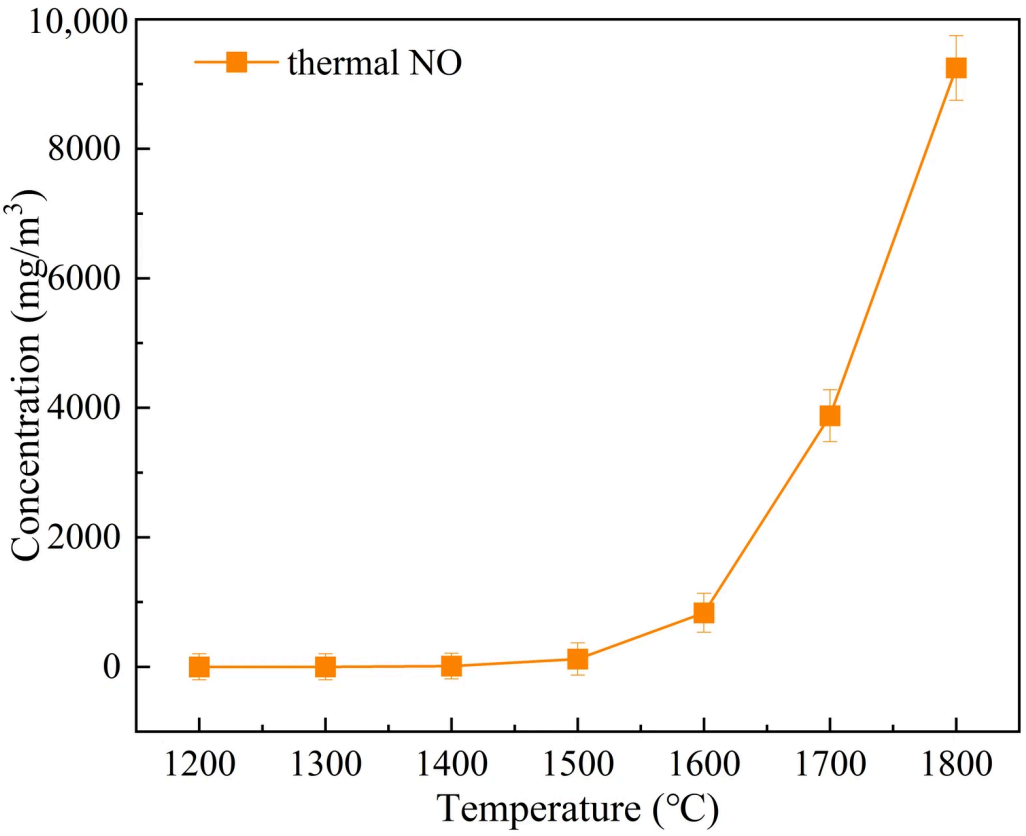


Figure 2. Variation in thermally generated NO concentration with temperature.

(2) Thermal Equilibrium Characteristics of NOx

To further elucidate the thermal equilibrium behavior of NOx and establish connections with laboratory experiments and engineering applications, the analysis was conducted from four perspectives: (i) the relationship between thermal equilibrium direction and temperature, (ii) the variation in thermal reduction efficiency with temperature for different initial NO concentrations, (iii) the relationship between reduction efficiency and injected NO concentration at a specific temperature, and (iv) the thermal equilibrium concentration as a function of temperature.

The thermal NO decomposition model was employed to inject NO into air at molar concentrations ranging from 0.015% to 10%, and the equilibrium concentrations obtained at different temperatures were subsequently determined. For high-concentration NO (e.g., 10%), as illustrated in Figure 3a, the concentration remained nearly constant below 1400 °C, indicating negligible thermal decomposition. Beyond 1400 °C, the concentration decreased continuously, with increasingly pronounced reductions at higher temperatures. At approximately 2000 °C, the concentration converged to values comparable to those obtained for low-concentration cases, suggesting that the equilibrium state became independent of the initial concentration.

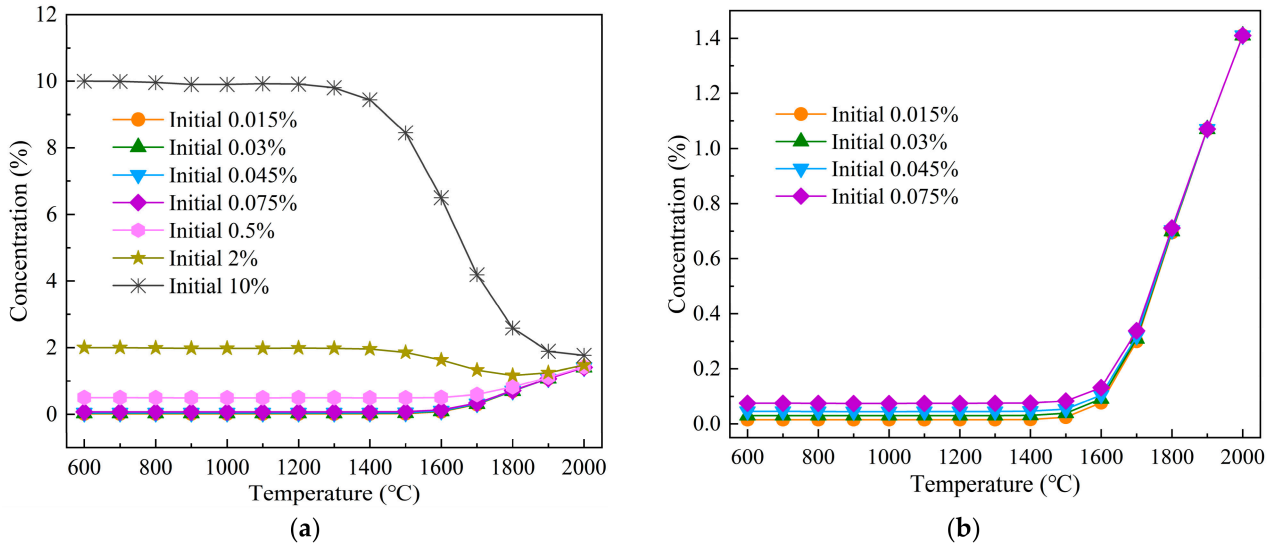


Figure 3. Relationship between thermal equilibrium direction and temperature for (**a**) high-concentration and (**b**) low-concentration NO.

To further investigate low-concentration behavior, simulations were conducted for initial concentrations of 0.015%, 0.03%, 0.045%, and 0.07%, as shown in Figure 3b. Similar to the high-concentration cases, the NO concentrations remained essentially unchanged below 1400 °C. However, above this temperature, the concentrations increased continuously and gradually converged near 1800 °C, indicating that thermal NO formation dominated under these conditions. The combined results demonstrate that thermal NO behavior is governed by the coexistence of formation and decomposition processes. Below 1400 °C, neither process is sufficiently active to alter the initial concentration significantly. Above 1400 °C, thermal formation dominates at low initial concentrations, whereas thermal decomposition prevails at high concentrations. At sufficiently high temperatures, both regimes converge toward a common equilibrium concentration that is independent of the initial NO concentration. Since the equilibrium concentration varies with temperature, further analysis is required to determine the concentration corresponding to zero net reduction at each temperature.

Based on the thermal NO decomposition model, representative high- and low-concentration cases within the range of 0.015–10% were analyzed, and the corresponding reduction efficiencies were calculated, as illustrated in Figure 4. For high-concentration NO (represented by an initial concentration of 10%), the reduction efficiency remained positive throughout the investigated temperature range up to 2000 °C. In contrast, for low-concentration NO (represented by an initial concentration of 0.5%), the reduction efficiency became negative at approximately 1500 °C and decreased further with increasing temperature. These findings indicate that a specific thermal equilibrium concentration exists at each temperature. When the injected NO concentration exceeds this equilibrium value, thermal decomposition dominates and the reduction efficiency is positive. Conversely, when the concentration falls below the equilibrium value, thermal formation becomes dominant, resulting in negative reduction efficiencies.

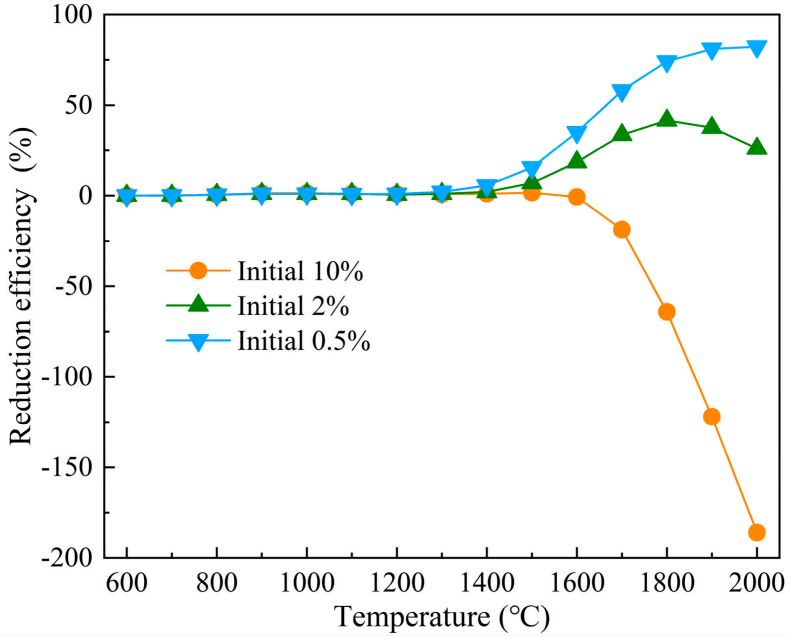


Figure 4. Variation in thermal reduction efficiency with temperature for different initial NO concentrations.

To quantitatively characterize the relationship between reduction efficiency and injected NO concentration, simulations were performed at 1500 °C using NO concentrations ranging from 0.0075% to 10%. The corresponding results are presented in Figure 5. The relationship between the test number on the horizontal axis and the injected NO concentration is listed in Table 1. When the injected concentration was below 0.357% (equivalent to 4781 mg·m^{-3}), the reduction efficiency remained negative. For example, an injection concentration of 0.0075% (100 mg·m^{-3}) yielded a reduction efficiency of −120%, indicating that thermal formation was dominant. Once the injected concentration exceeded 0.357%, the reduction efficiency became positive. At an injection concentration of 0.5% (6696 mg·m^{-3}), the reduction efficiency reached only 1.3%, suggesting that thermal decomposition had become dominant but remained relatively weak.

Accordingly, the critical concentration corresponding to zero reduction efficiency at 1500 °C was determined to be 0.357% (4781 mg·m^{-3}), which represents the thermal equilibrium concentration of NO at this temperature. However, even when the injected concentration increased to 1% (13,393 mg·m^{-3}), the reduction efficiency remained only 3.9%, indicating that purely thermal reduction under conventional high-temperature conditions is inherently limited. The methodology employed to determine this critical concentration can readily be extended to other temperatures, thereby providing a basis for subsequent tubular

furnace experiments and for evaluating the contribution of thermal reduction mechanisms in practical applications.

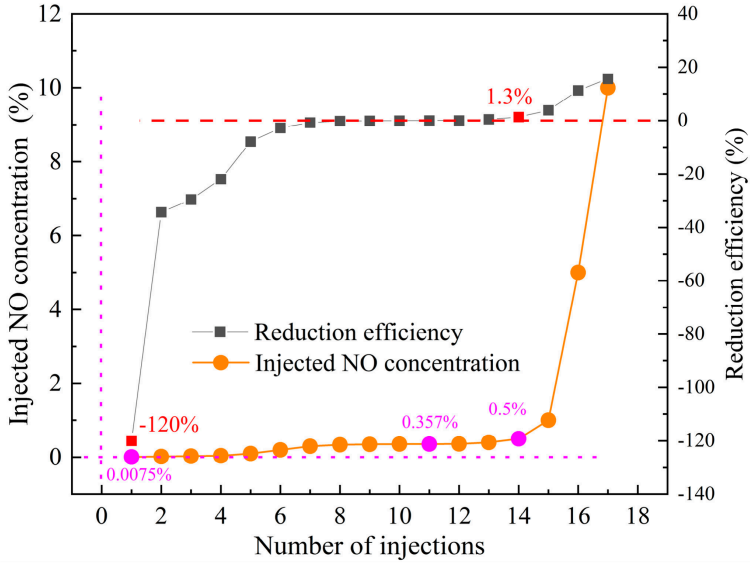


Figure 5. Relationship between reduction efficiency and injected NO concentration at 1500 °C.

Table 1. The relationship between the test number on the horizontal axis and the injected NO concentration.

Test No.	1	2	3	4	5	6	7	8	9	10	11	12	13	14	15	16	17
Injected concentration (%)	0.01	0.02	0.03	0.04	0.10	0.20	0.30	0.34	0.35	0.36	0.36	0.36	0.40	0.50	1.00	5.00	10.00

(3) Relationship between Thermal Equilibrium Concentration and Temperature

The pure thermal NO decomposition model was further employed to determine the equilibrium concentration corresponding to zero net reduction efficiency for initial NO concentrations ranging from 0.015% to 10%. The resulting thermal equilibrium concentrations at different temperatures are shown in Figure 6.

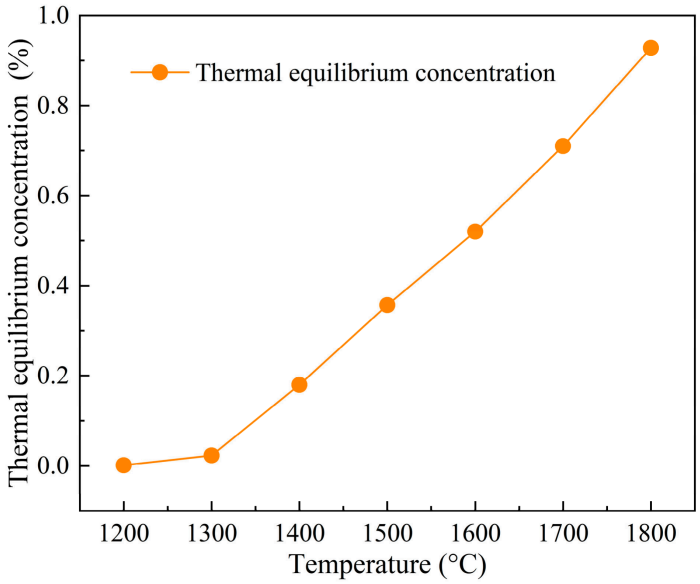


Figure 6. Relationship between thermal equilibrium concentration and temperature.

The thermal equilibrium concentration increased continuously with temperature. Specifically, the equilibrium concentration was 0.0013% (17 mg·m^{-3}) at 1200 °C, 0.357% (4781 mg·m^{-3}) at 1500 °C, and 0.928% (12,428 mg·m^{-3}) at 1800 °C. This equilibrium curve effectively distinguishes the relative dominance of thermal formation and thermal decomposition processes. At a given temperature, when the injected NO concentration is lower than the corresponding equilibrium value, thermal formation predominates, resulting in outlet concentrations higher than inlet concentrations and consequently negative reduction efficiencies. Conversely, when the injected concentration exceeds the equilibrium value, thermal decomposition becomes dominant, yielding positive reduction efficiencies. The equilibrium concentration–temperature relationship presented in Figure 5 provides an important reference for the design and interpretation of subsequent tubular furnace experiments.

(4) Reburning Reduction Characteristics of NO under Reducing Atmospheres

To further investigate the reburning reduction behavior of NO under reducing conditions, the analysis focused on four aspects: (i) the influence of reducing atmosphere intensity on the equilibrium concentration of reburned NO, (ii) the temporal characteristics of the reburning process, (iii) reduction efficiencies at different initial NO concentrations, and (iv) the synergistic mechanisms of individual reducing species, namely CO, H_2, and CH_4. In accordance with practical engineering conditions, the temperature range considered in this section was 1100–1800 °C. Using the thermal decomposition and reduction model for recycled NO, initial NO concentrations ranging from 0.02% to 1% were introduced into a strongly reducing atmosphere containing 8.0% CO, 4.0% H_2, and 2.0% CH_4. The equilibrium concentrations obtained at different temperatures are illustrated in Figure 7a.

Under strongly reducing conditions, the equilibrium concentrations decreased continuously with increasing temperature for all initial NO concentrations, with more pronounced reductions observed at higher initial concentrations. Beyond 1400 °C, the decreasing trend gradually leveled off. For example, for an initial concentration of 1%, the equilibrium concentration decreased from 0.35% at 1100 °C to 0.07% at 1300 °C and further to 0.04% at 1500 °C, remaining nearly constant thereafter. Corresponding simulations under a weakly reducing atmosphere, consisting of 3.0% CO, 2.0% H_2, and 0.5% CH_4, are presented in Figure 7b. The reduction in equilibrium concentration was noticeably slower than that observed under strongly reducing conditions. For an initial NO concentration of 1%, the equilibrium concentration decreased from 0.45% at 1100 °C to 0.19% at 1300 °C and to 0.12% at 1500 °C, followed by a gradual decline at higher temperatures.

A direct comparison between strong and weak reducing atmospheres is shown in Figure 7c. For example, at an initial concentration of 0.04% and a temperature of 1100 °C, the equilibrium concentration under strongly reducing conditions was 0.15%, compared with 0.21% under weakly reducing conditions, indicating superior NO reduction performance in the former case. These results demonstrate that both thermal effects and reducing atmospheres contribute to NO reduction, whereas strong reducing atmospheres provide substantially greater enhancement. Combined with the thermal equilibrium behavior presented in Figure 3, it can be further concluded that reducing atmospheres enable effective NO reduction at significantly lower temperatures. For instance, for an initial NO concentration of 0.4%, the concentration remains essentially unchanged below 1300 °C in a purely thermal system, whereas under strongly reducing conditions, it decreases to approximately 0.03% at the same temperature.

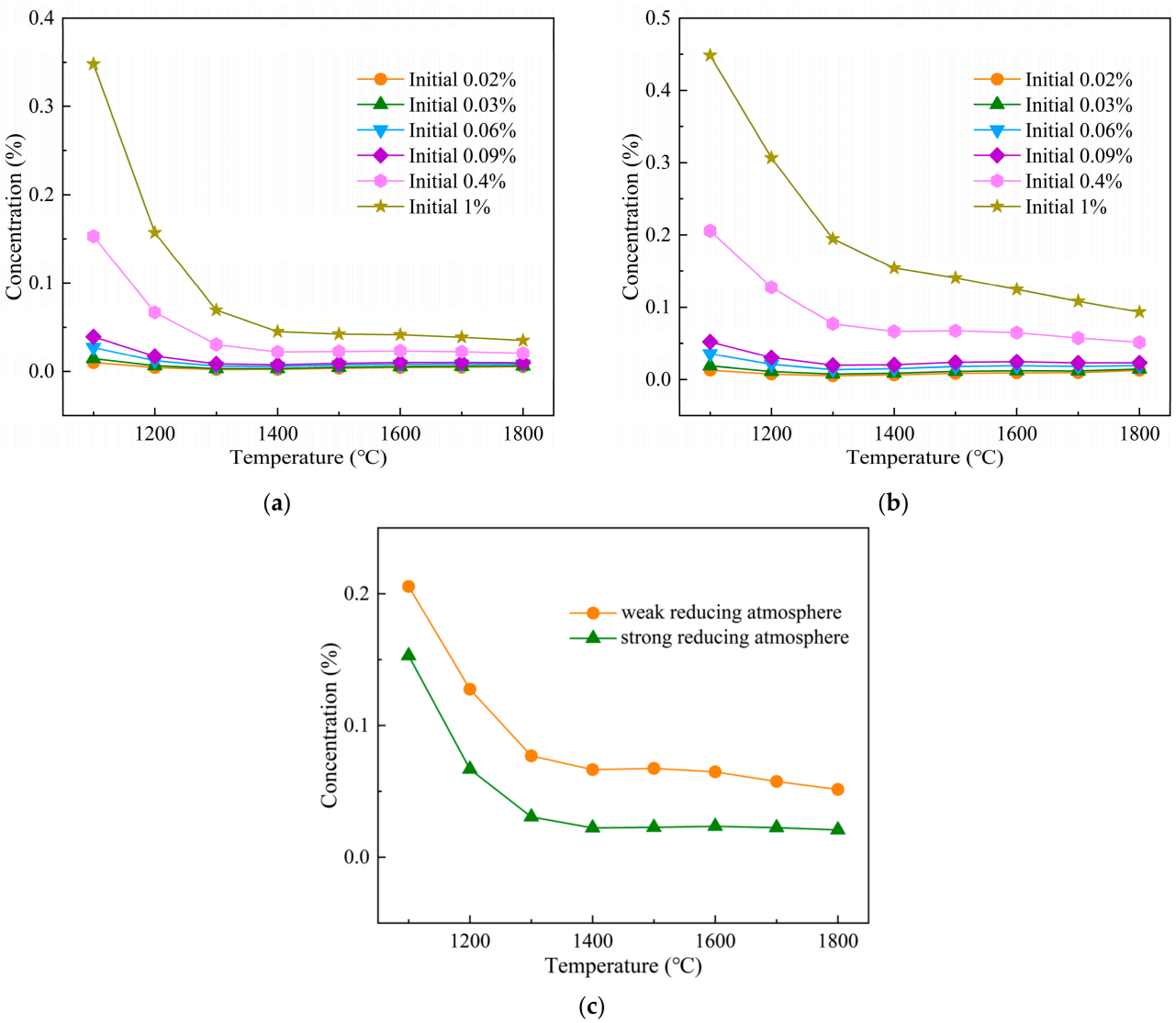


Figure 7. Reburning reduction characteristics of NO under reducing atmospheres: (**a**) strong reducing atmosphere, (**b**) weak reducing atmosphere, and (**c**) comparison between the two conditions.

The thermal decomposition and reduction model was further employed to investigate the influence of residence time on NO reburning behavior. Initial NO concentrations ranging from 0.02% to 1% were introduced into high-temperature, strongly reducing atmospheres, and the instantaneous concentrations after 2.5 s of reaction were calculated. The results for the representative case of an initial concentration of 1% are compared with the corresponding equilibrium concentrations in Figure 8. At temperatures below 1200 °C, a pronounced delay in the reburning process was observed, and equilibrium could not be reached within 2.5 s. In contrast, at temperatures above 1200 °C, reaction rates increased substantially, enabling the system to attain equilibrium within the same residence time. These findings indicate that residence time is a critical factor governing NO reburning efficiency under low-temperature conditions. In practical boiler applications, where residence times within reburning zones may range from only 0.5 to 1.5 s, this effect cannot be neglected. However, as temperature increases, the influence of residence time gradually diminishes and eventually becomes negligible. This observation provides important theoretical guidance for the design of residence times in engineering reburning systems.

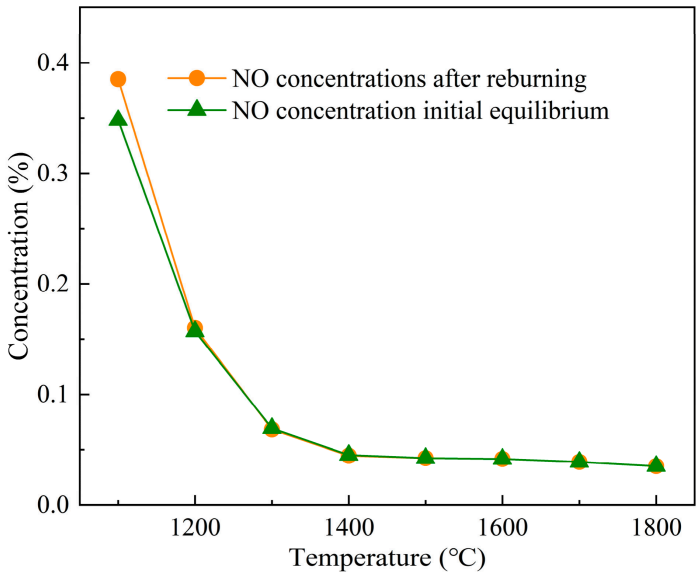


Figure 8. Comparison between NO concentrations after 2.5 s of reburning and their equilibrium values for an initial NO concentration of 1%.

Simulations were performed under strongly reducing conditions for initial NO concentrations ranging from 0.02% to 1%, corresponding to typical boiler operating scenarios. The equilibrium concentrations obtained after thermal decomposition and reduction were used to calculate NO reduction efficiencies, as shown in Figure 9. Overall, the reduction efficiency increased with temperature for all initial concentrations, rising from approximately 60% at 1100 °C to around 90% at 1300 °C, after which distinct behaviors emerged. For high-concentration NO (1%), the reduction efficiency increased rapidly from 65% at 1100 °C to 95% at 1400 °C and then gradually approached 97% at 1800 °C. For medium-concentration NO (0.09%), the reduction efficiency rose from 56% at 1100 °C to 92% at 1400 °C, followed by a slight decline to 89% at 1800 °C. For low-concentration NO (0.02%), the reduction efficiency increased from 50% at 1100 °C to 88% at 1300 °C but subsequently decreased gradually to 79% at 1800 °C.

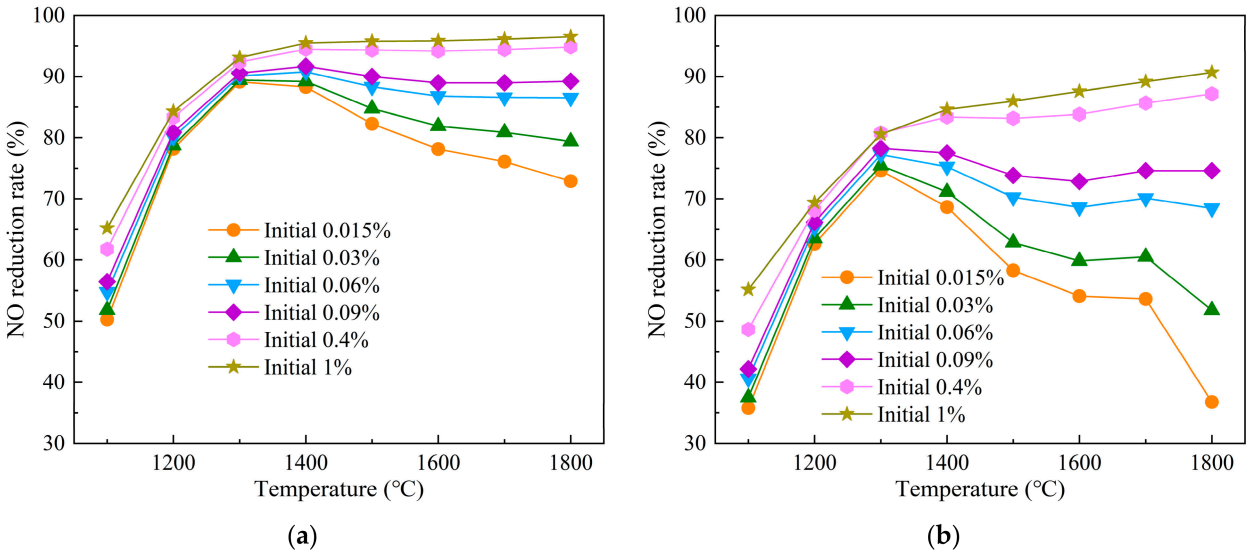


Figure 9. NO reduction rate curves at various concentrations: (**a**) Under a highly reducing atmosphere. (**b**) Under a low-reducing atmosphere.

These results indicate that strongly reducing atmospheres can achieve remarkably high NO reburning efficiencies, with a common optimal temperature window of 1250–1450 °C, within which reduction efficiencies of 70–90% can be attained regardless of the initial concentration. Above 1450 °C, however, the continuous generation of background thermal NO begins to offset the reburning reduction effect, and this influence becomes increasingly significant at lower NO concentrations. Consequently, while high-concentration NO continues to exhibit slight improvements in reduction efficiency, low-concentration NO experiences a gradual decline. Regardless of the reducing atmosphere intensity, the temperature interval of 1250–1450 °C consistently represents the optimum operating window for NO reburning. Furthermore, increasing the concentration of reducing species constitutes an effective strategy for enhancing NO reduction performance under identical thermal conditions.

Further tracking of species evolution data obtained from CHEMKIN simulations indicates that among the main reducing species (CO, H_2, and CH_4), only H_2 and CH_4 directly participate in NO decomposition reactions. Their concentrations decrease rapidly from the order of 10^{-2} to approximately 10^{-7} during the NO reduction process. In contrast, the concentration of CO gradually increases and remains within the same order of magnitude throughout the reaction. This phenomenon suggests that, in the presence of strongly reducing species such as H_2 and CH_4, CO primarily contributes indirectly by maintaining a reducing (oxygen-deficient) atmosphere rather than directly participating in NO reduction reactions. (The independent role of CO will be further verified in Section 3.2 through chemical model calculations and one-dimensional furnace experiments.) These findings are consistent with theoretical analysis and confirm a free-radical–driven, multi-component synergistic reaction network governing NO reduction.

(4) Determination of Key Engineering Parameters
Based on the computational results of Models IV–VI, recommended parameter ranges for NO reburning treatment in different furnace types were obtained as follows:

(a) Pulverized coal furnace:
Reburning zone temperature: 1200–1500 °C; reducing agent concentrations: CO 3–8%, H_2 1–4%, CH_4 0.5–2%. Under these conditions, the NO reburning reduction efficiency can exceed 90% at equivalent NO concentrations.

(b) Plasma furnace:
Reburning zone temperature: 1400–1700 °C; higher reducing agent concentrations can be applied. The NO reburning reduction efficiency can reach approximately 95%.

(c) Gas-fired furnace:
Reburning zone temperature: 1100–1400 °C; CH_4 content has the most significant influence on reduction efficiency. The NO reburning reduction efficiency ranges from 70% to 85%.

3.2. Laboratory Tubular Furnace Validation Experiments

To verify the reliability of the above model predictions, a laboratory tubular furnace system was constructed, and experimental data were compared with simulation results to validate model accuracy.

(1) Experimental Validation of Thermal NOx Formation

To investigate thermal NOx formation characteristics, baseline experiments were conducted without NO injection. The total airflow rate was fixed at 180 mL/min, and the gas residence time in a 150 mm heated tube was approximately 15 s. A synthetic air atmosphere was prepared with O_2 (21 vol%) and N_2 (79 vol%). The furnace temperature was increased from 800 °C to 1700 °C in 100 °C increments, and NOx concentrations at the outlet were

measured at each temperature. After stabilization, data were recorded continuously for 30 min at each temperature point, and the average value was taken as the NOx formation level. Figure 10 compares CHEMKIN simulation results with experimental measurements. Both approaches show zero NO concentration in the range of 800–1200 °C. Trace NO begins to appear above 1300 °C, reaching approximately 14 mg/m^3 at 1400 °C. At 1500 °C, simulated and experimental values are 120 mg/m^3 and 114 mg/m^3, respectively. At 1600 °C, values increase to 834 mg/m^3 (simulation) and 920 mg/m^3 (experiment). At 1700 °C, NO concentrations reach 3877 mg/m^3 (0.29%) and 3708 mg/m^3 (0.28%), respectively.

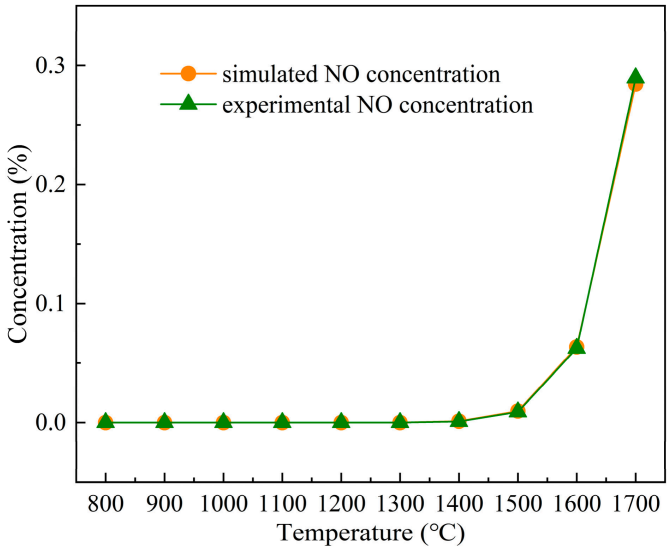


Figure 10. Comparison of simulated and experimental NO concentration generated by thermal process.

The simulation results agree well with experimental data, with a coefficient of determination $R^2 > 0.98$, confirming the high accuracy of the proposed model. Both simulation and experimental results demonstrate that thermal NO formation increases with temperature and exhibits exponential growth above 1500 °C.

(2) Experimental Validation of Thermal NO Reduction

To further investigate NO reduction behavior at high temperatures and clarify the relationship between reduction efficiency and inlet concentration at 1500 °C, NO was injected into the system at concentrations ranging from 0.0075% to 10%, based on simulation-derived conditions. After stabilization, outlet NO concentrations were recorded over 30 min and averaged to calculate reduction efficiency.

The results show that when the inlet concentration approaches 0.357% (≈4750 mg/m^3), inlet and outlet concentrations become nearly equal. Below this threshold, outlet concentrations exceed inlet values (e.g., 100 mg/m^3 inlet corresponds to 210 mg/m^3 outlet). Above this threshold, outlet concentrations become lower than inlet values (e.g., 6696 mg/m^3 inlet corresponds to 6610 mg/m^3 outlet). The corresponding reduction efficiencies were calculated, as shown in Figure 11a. Starting from an inlet concentration of 0.075%, the reduction efficiency increases from a minimum negative value of −109% and approaches zero at approximately 0.1%. It becomes positive near 0.357% and continues to increase, reaching 4.05% at 1%. These results indicate that the tubular furnace experiment can effectively characterize NO thermal decomposition behavior and that experimental data are directly comparable with CHEMKIN simulations. Furthermore, a positive correlation between inlet concentration and reduction efficiency is confirmed: at low inlet concentrations, outlet concentrations exceed inlet values (negative efficiency), whereas above a critical concentration,

reduction becomes positive. Comparison between simulated and experimental reduction efficiency curves at 1500 °C shows strong agreement as exhibited in Figure 11b. For example, at 0.02% inlet concentration, simulated and experimental efficiencies are −34.32% and −30.67%, respectively. At 0.5%, values are 1.34% and 1.29%, respectively. Near the threshold concentration (~0.357%), both approach zero. Below this value, efficiencies are negative and decrease rapidly with decreasing concentration; above it, efficiencies become positive and increase gradually.

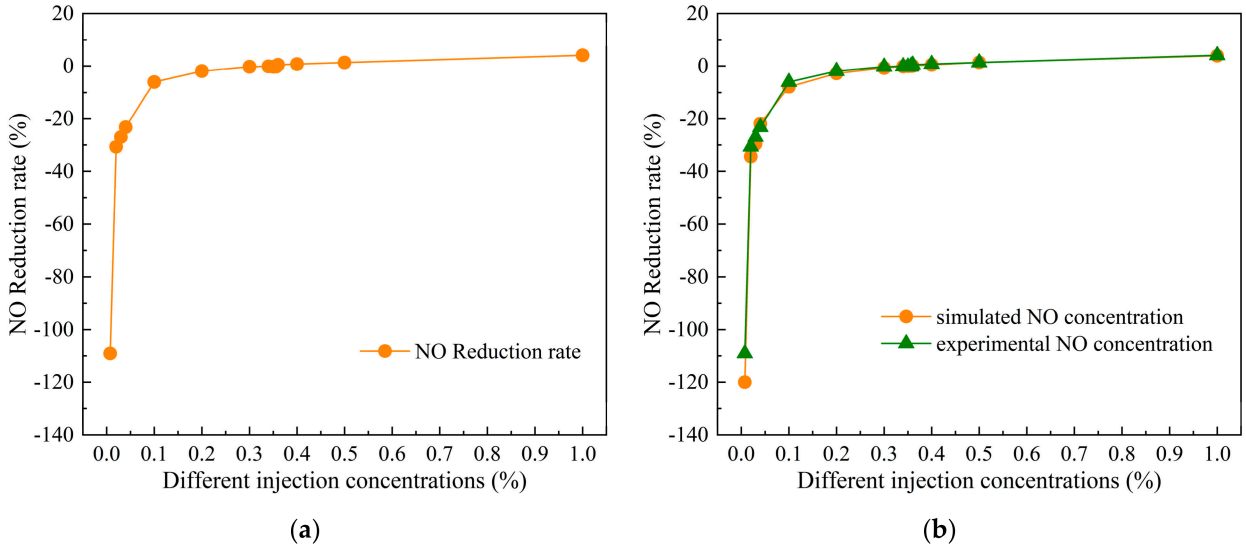


Figure 11. Experimental Validation of Thermal NO Reduction: (**a**) NO Reduction rate corresponding to different injection concentrations in the laboratory tubular furnace. (**b**) Comparison of NO reduction rates under simulated and experimental thermal conditions.

A critical concentration of 0.357% (≈4781 mg/m^3) exists at 1500 °C. Below this value, NO exhibits net formation (negative reduction efficiency), while above it, net reduction occurs. Even at 1% inlet concentration (≈13,393 mg/m^3), the reduction efficiency remains low (3.90–4.05%), indicating limited pure thermal reduction capability. The close agreement between simulation and experiment further validates the model.

(3) NO Reburning Reduction under Reducing Atmosphere

A reducing atmosphere dominated by CO was established by continuously introducing a gas mixture composed of 3% CO, 19.49% CO_2, 0.01% O_2, and 77.47% N_2. NO with an initial concentration of 0.03% was simultaneously injected. Outlet NO concentrations were recorded over a temperature range of 1100–1700 °C (100 °C intervals). Experimental results are summarized in Table 2. Corresponding simulation conditions were input into the CHEMKIN-based NO reburning model to calculate reduction efficiencies, as shown in Table 3.

Table 2. Experimental Data of NO Reburning in Tubular Furnace.

Temperature (°C)	Inlet NO (mg/m^3)	Inlet NO (%)	Outlet NO (mg/m^3)	Outlet NO (%)	Reduction Efficiency (%)
1100	401.8	0.03%	381	0.0285%	5.09%
1200	401.8	0.03%	364	0.0271%	9.52%
1300	401.8	0.03%	333	0.0249%	17.04%
1400	401.8	0.03%	307	0.0229%	23.65%
1500	401.8	0.03%	285	0.0213%	29.01%
1600	401.8	0.03%	256	0.0191%	36.33%
1700	401.8	0.03%	263	0.0196%	34.66%

Table 3. Simulated NO Reburning Results (CHEMKIN Model).

Temperature (°C)	Inlet NO (mg/m³)	Inlet NO (%)	Outlet NO (mg/m³)	Outlet NO (%)	Reduction Efficiency (%)
1100	401.8	0.03%	379	0.0283%	5.65%
1200	401.8	0.03%	361	0.0269%	10.18%
1300	401.8	0.03%	337	0.0252%	16.04%
1400	401.8	0.03%	311	0.0232%	22.65%
1500	401.8	0.03%	284	0.0212%	29.34%
1600	401.8	0.03%	260	0.0194%	35.26%
1700	401.8	0.03%	260	0.0194%	35.28%

Figure 12 compares experimental and simulated NO reburning efficiencies. The results show excellent agreement, with experimental points closely following the simulation curve. The reduction efficiency increases with temperature and reaches a maximum around 1600 °C, after which it slightly decreases. Specifically, at 1100 °C, simulated and experimental efficiencies are 5.65% and 5.09%, respectively; at 1400 °C, 22.65% and 23.65%; and at 1600 °C, 35.26% and 36.33%. These results demonstrate that experimental measurements under a CO-based reducing atmosphere validate the CHEMKIN simulations. Both indicate that the reburning efficiency of low-concentration NO peaks near 1600 °C and then decreases due to enhanced formation of thermal NO at higher temperatures.

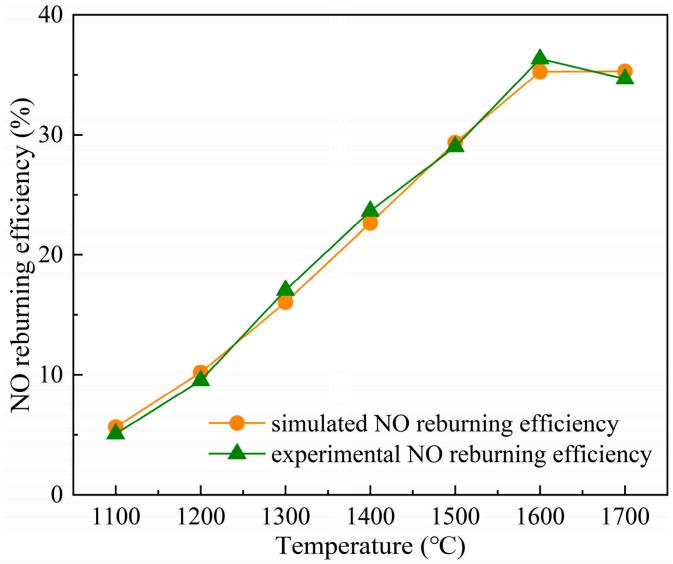


Figure 12. Comparison of Simulated and Experimental NO Reburning Efficiency at 0.03% Inlet Concentration.

Owing to the explosion risk of multi-component flammable gases at high temperatures, the reducing-atmosphere validation was deliberately limited to a CO-dominated mixture; nevertheless, the good agreement between the measured and simulated CO-only reduction efficiencies provides preliminary validation of the model framework. This conclusion further supports the simulated synergistic mechanism of reducing agent components, indicating that CO alone provides limited NO reduction capability, while the synergistic promotion by H_2 and CH_4 remains to be further verified experimentally.

4. Conclusions

This study developed six chemical kinetic reactor models to systematically investigate thermal NOx formation and decomposition as well as NO reburning behavior under

reducing atmospheres. The models were validated through laboratory tubular furnace experiments. The main conclusions are as follows:

(1) The thermal-NO equilibrium is integrated into the proposed reburning–equilibrium framework as a constraint governing the net direction of NO conversion rather than as a restatement of the conventional temperature-dependent generation trend. The coupled model–experiment–pilot–engineering validation shows that purely thermal reduction is insufficient for high-concentration NOx disposal, which establishes the need to shift from thermal-equilibrium control to reducing-atmosphere-enhanced reburning. This provides the criterion for designing the integrated COAP route for high-concentration NOx disposal.

(2) Existence of thermal NO equilibrium: NO formation and decomposition reach a temperature-dependent equilibrium. Below 1400 °C, equilibrium effects are negligible; above this temperature, they become increasingly significant and dominate near 2000 °C. At a given temperature, inlet concentrations above the equilibrium value lead to net decomposition (positive reduction efficiency), while concentrations below it result in net formation (negative reduction efficiency). At 1500 °C, the equilibrium concentration is 4781 mg/m^3. Even at 13,393 mg/m^3, the net thermal reduction efficiency remains low (~4%), indicating limited effectiveness of pure thermal processes.

(3) Enhancement of NO reduction by reducing atmospheres: Within 1250–1450 °C under strongly reducing conditions, NO reduction efficiency can reach 70–90%. The synergistic effects among reducing agents are significant: CH_4 acts as a radical initiator and has the strongest influence on efficiency, H_2 participates directly in reduction reactions, and CO primarily maintains a reducing atmosphere and indirectly promotes NO reduction.

Author Contributions: Conceptualization, S.W.; methodology, X.Q.; software, Y.W.; validation, P.L.; formal analysis, T.L.; investigation, X.Q.; resources, P.X.; data curation, Y.W.; writing—original draft preparation, S.W.; writing—review and editing, P.L.; visualization, T.L.; supervision, H.Z.; project administration, P.X.; funding acquisition, H.Z. All authors have read and agreed to the published version of the manuscript.

Funding: This research was funded by the National Key Research and Development Program, grant number 2022YFB4100200.

Data Availability Statement: The original contributions presented in this study are included in the article. Further inquiries can be directed to the corresponding author.

Acknowledgments: This work was sponsored by the National Key Research and Development Program (2022YFB4100200).

Conflicts of Interest: Authors Shiqing Wang and Yutong Wang were employed by State Key Laboratory of High-Efficiency Flexible Coal Power Generation and Carbon Capture Utilization and Storage, China Huaneng Group. Huadong Zhang was employed by Huaneng Linyi Power Generation Co., Ltd. Xiaolong Qiu and Ping Xiao were employed by Huaneng Clean Energy Research Institute. The remaining authors declare that the research was conducted in the absence of any commercial or financial relationships that could be construed as a potential conflict of interest.

References

1. Dai, G.; Liu, B.; Wang, R.; Wang, H.; Miao, Y.; Hou, S.; Lian, D.; Chen, M.; Li, C.; Zhang, Z.; et al. Pretreatment techniques in CO-SCR and NH_3-SCR: Status, challenges, and perspectives. *J. Catal.* **2025**, *442*, 115925. [CrossRef]
2. Elkaee, S.; Phule, A.D.; Yang, J.H. Advancements in (SCR) technologies for NOx reduction: A comprehensive review of reducing agents. *Process Saf. Environ. Prot.* **2024**, *184*, 854–880. [CrossRef]
3. Song, K.L.; Feng, X.B.; Zhang, N.; Ma, D.D.; Shi, L.; Chen, Y.; Li, J.; Shi, J.W. Metal-organic framework materials in NH_3-SCR: Progress and prospects. *Coord. Chem. Rev.* **2025**, *535*, 216615. [CrossRef]

4. Zhang, X.L.; Wang, Y.; Jin, S.; Wang, X.Y.; Wang, K.; Chen, Y.Z.; Wu, X.P. Enhanced NH_3-SCR 3-SCR performance using hydrothermally synthesized cell-like MnOx x loaded rectorite catalysts. *Appl. Catal. O OPEN* **2024**, *194*, 207004. [CrossRef]
5. Zhao, J.Y.; Zhang, X.G.; Yang, F.H.; Ai, Y.H.; Chen, Y.S.; Pan, D. Strategy and Technical Progress of Recycling of Spent Vanadium-Titanium-Based Selective Catalytic Reduction Catalysts. *Acs Omega* **2024**, *9*, 6036–6058. [CrossRef] [PubMed]
6. Ren, S.; Li, X.D.; He, C.; Chen, L.; Wang, L.; Li, F.G. Surface tailoring on bifunctional CuOx/MnO_2 catalyst to promote the selective catalytic reduction of NO with NH_3 and oxidation of CO with O_2. *Sep. Purif. Technol.* **2024**, *346*, 127471. [CrossRef]
7. Chen, Z.J.; Li, Z.; Hu, X.Y.; Wang, Z.J.; Yang, H.Y.; Elsharkawy, E.R.; El-Bahy, S.M.; Wu, M.M.; Hu, M.M.; Guo, Z.H. Simulation and experiment on improving NOX conversion efficiency of ship selective catalytic reduction system. *Alex. Eng. J.* **2024**, *103*, 237–250. [CrossRef]
8. Yang, Z.D.; Song, J.Y.; Zhang, G.M.; Sun, X.; Cheng, S.Y.; Zhang, X.; Jiang, Y. Unraveling the promotion for SO_2 and H_2O resistance of transition metal-doped CeO_2-TiO_2 catalysts in NH_3-SCR reaction: A DFT study. *J. Hazard. Mater.* **2025**, *489*, 137563. [CrossRef] [PubMed]
9. Lin, K.X.; Feng, X.B.; Zhang, N.; Song, K.L.; Yao, Y.Y.; Jiao, R.Q.; Chen, Y.; Shi, L.; Shi, J.W. Recent progress in layered double hydroxides-derived catalysts for selective reduction of nitrogen oxides by ammonia. *Sci. China-Chem.* **2025**, *68*, 4642–4676. [CrossRef]
10. Chen, Z.G.; Liu, Q.Y.; Liu, H.Y.; Wang, T.Y. Recent Advances in SCR Systems of Heavy-Duty Diesel Vehicles-Low-Temperature NOx Reduction Technology and Combination of SCR with Remote OBD. *Atmosphere* **2024**, *15*, 997. [CrossRef]
11. Niu, K.; Liu, Q.L.; Liu, C.X.; Yu, Z.H.; Zheng, Y.F.; Su, Y.; Zhao, Y.J.; Liu, B.Q.; Cui, S.P.; Zang, G.L.; et al. Unraveling the role of oxygen vacancies in metal oxides: Recent progress and perspectives in NH 3-SCR for NOx removal. *Chem. Eng. J.* **2024**, *487*, 150714. [CrossRef]
12. Xu, Y.Y.; Peng, L.; Wei, J.L.; Liao, Y.Z. Ammonia coverage ratio control of a novel two-cell SCR-DeNOX system configuration based on IA-ISMC. *Chem. Eng. Sci.* **2024**, *295*, 120148. [CrossRef]
13. Liu, J.H.; Pan, Y.; Duan, Y.J.; Liang, S.Q.; Cheng, H.F.; Hua, M.Q.; Dai, X.H.; Liu, F.; Li, H.M.; Liu, J.X. Fe1-yMnyZr$_4$Ox solid solution for efficient low-temperature selective catalytic reduction of NOx. *Chem. Eng. Sci.* **2025**, *313*, 121750. [CrossRef]
14. Feng, X.B.; Zhu, J.R.; Song, K.L.; Zeng, J.L.; Zhou, X.Y.; Lin, K.X.; Guo, X.L.; Zhang, C.H.; Xie, C.; Shi, J.W. Insight into the reasons for enhanced NH_3-SCR activity and SO_2 tolerance of Mn-Co layered oxides. *Sep. Purif. Technol.* **2024**, *336*, 126285. [CrossRef]
15. Gao, M.; Lu, G.G.; Li, Z.C.; Wang, X.; Duan, R.C.; Fu, Y.; He, G.Z.; He, H. Unveiling the Reaction Mechanism of Selective Catalytic Reduction of NO with NH_3 over Active Mn-W Dinuclear Sites. *Environ. Sci. Technol.* **2025**, *59*, 19060–19067. [CrossRef] [PubMed]
16. Zhu, J.Y.; Jin, C.; Duan, Y.J.; Zhu, L.H.; Liu, J.H.; Cheng, K.; Cheng, H.F.; Liu, F.; Li, H.M.; Liu, J.X. Fe-triggered Mn-mullite oxides for efficient low-temperature reduction of nitrogen oxides: Insights into the structure-activity relationship. *Appl. Catal. B-Environ. Energy* **2025**, *366*, 125028. [CrossRef]
17. Yang, J.; Zhou, H.; Luo, Y.; Cheng, Y.L.; Wang, S.; Yao, L.; Wan, Y.D.; Zhu, J.J. Insight into the promotion effects of Ce on the performances of V-Ti based catalyst for low-temperature NH_3-SCR: In-situ spectroscopy studies. *Sep. Purif. Technol.* **2025**, *362*, 131714. [CrossRef]
18. Han, X.Y.; Liu, K.J.; Bian, M.Y.; Yuan, Z.X.; Li, Y.N.; Zhang, Y.L.; Yang, X.G.; Zhang, Y.B. SO_2-induced surface defects on monatomic Ce-doped MoTiOx catalyst for efficient reduction of NOx with NH_3. *Appl. Catal. B-Environ. Energy* **2025**, *366*, 125021. [CrossRef]
19. Jia, L.F.; Zhang, L.; Liu, B.; Cheng, H.F.; Li, H.Q.; Zhao, Z.; Zhu, W.S.; Song, W.Y.; Liu, J.; Liu, J.X. Interface Induced by Hydrothermal Aging Boosts the Low-Temperature Activity of Cu-SSZ-13 for Selective Catalytic Reduction of NOx. *Environ. Sci. Technol.* **2024**, *58*, 15038–15051. [CrossRef] [PubMed]
20. Zhuang, Z.Q.; Guan, B.; Chen, J.Y.; Zheng, C.Z.; Zhou, J.F.; Su, T.X.; Chen, Y.J.; Zhu, C.Y.; Hu, X.H.; Zhao, S.K.; et al. Review of nitrous oxide direct catalytic decomposition and selective catalytic reduction catalysts. *Chem. Eng. J.* **2024**, *486*, 150374. [CrossRef]
21. Song, K.L.; Feng, X.B.; Ju, X.Q.; Ma, D.D.; Wang, S.B.; Shi, J.W. Poisoning mechanism of potassium and calcium on a Mn-based quasi-MOF de-NOx catalyst. *J. Hazard. Mater.* **2025**, *497*, 139714. [CrossRef] [PubMed]
22. Zheng, D.Y.; Liu, K.J.; Zhang, Z.S.; Fu, Q.; Bian, M.Y.; Han, X.Y.; Shen, X.; Chen, X.H.; Xie, H.J.; Wang, X.; et al. Essential features of weak current for excellent enhancement of NOx reduction over monoatomic V-based catalyst. *Nat. Commun.* **2024**, *15*, 6688. [CrossRef] [PubMed]
23. Ma, X.J.; Qiu, T.; Lei, Y.; Chen, Z.X. Real-time emission test and evaluation method of heavy-duty diesel vehicle SCR system based on dynamic time warping. *Int. J. Heavy Veh. Syst.* **2025**, *32*, 304–326. [CrossRef]
24. Zhang, Z.Q.; Li, D.M.; Lan, G.L.; Yin, Z.B.; Pan, M.Z.; Jiang, F.; Li, J.M.; Tan, D.L. Development and evaluation of mechanistic model for standard SCR, fast SCR, and NO_2 SCR of NH_3-SCR over Cu-ZSM-5. *Energy* **2024**, *306*, 132544. [CrossRef]
25. Kose, S. NOx emission reduction in tugboats with SCR systems: Real-world impact of AdBlue. *Sustain. ENERGY Technol. Assess.* **2025**, *76*, 104309. [CrossRef]
26. Xu, Y.; Tan, C.; Wang, Y.; Zhu, B.Y.; Gu, Z.W.; Sin, S.; Huang, C.K.; Hao, S.J.; Zhang, Q.; Xu, J.X.; et al. Regeneration of sulfur-poisoned CeO_2 catalysts via in situ treatment from NH_3-SCR atmosphere. *J. Environ. Chem. Eng.* **2024**, *12*, 114432. [CrossRef]

27. Duan, R.C.; Li, Z.C.; Fu, Y.; Shan, Y.L.; Yu, Y.B.; He, G.Z.; He, H. Combined Experimental and Density Functional Theory Study on the Mechanism of the Selective Catalytic Reduction of NO with NH_3 over Metal-Free Carbon-Based Catalysts. *Environ. Sci. Technol.* **2024**, *58*, 5598–5605. [CrossRef] [PubMed]
28. Zhang, W.; Huang, K.N.; Chen, Z.H.; Li, Z.H.; Zhou, M.Y. Mechanistic study of SCR (NH_3-fast-SCR) for NOx removal from ammonia-hydrogen engine by single-atom Fe-beta zeolite. *Fuel* **2026**, *407*, 137343. [CrossRef]
29. Andana, T.; Rappe, K.G.; Gao, F.; Wang, Y. Mitigated ammonium nitrate inhibition in SCR over Cu-SSZ-13+Ce/Mn-oxide composite catalysts: Insights from temperature-programmed desorption analysis. *Catal. Sci. Technol.* **2024**, *14*, 2178–2191. [CrossRef]
30. Guan, B.; Chen, J.Y.; Zhuang, Z.Q.; Zhu, L.; Ma, Z.R.; Hu, X.H.; Zhu, C.Y.; Zhao, S.K.; Shu, K.Y.; Dang, H.T.; et al. Experimental Studies on NOx Removal and Soot Regeneration Characteristics of a Selective Catalytic Reduction Filter. *Ind. Eng. Chem. Res.* **2024**, *64*, 209–220. [CrossRef]
31. Duan, R.C.; Fu, Y.; Li, Z.C.; Wang, X.; Gao, M.; Yu, Y.B.; He, G.Z.; He, H. Unexpected Room-Temperature Selective Catalytic Reduction of NOx with NH_3 over Metal-Free Carbon-Based Catalysts. *Environ. Sci. Technol.* **2025**, *59*, 7760–7767. [CrossRef] [PubMed]
32. Fu, Y.; Sun, Y.; Shan, Y.L.; Chen, J.L.; Du, J.P.; He, G.Z.; He, H. Unexpected Promotion Effect of H_2O on the Selective Catalytic Reduction of NOx with NH_3 over Cu-SSZ-39 Catalysts. *Environ. Sci. Technol.* **2024**, *58*, 3520–3529. [CrossRef] [PubMed]

Disclaimer/Publisher's Note: The statements, opinions and data contained in all publications are solely those of the individual author(s) and contributor(s) and not of MDPI and/or the editor(s). MDPI and/or the editor(s) disclaim responsibility for any injury to people or property resulting from any ideas, methods, instructions or products referred to in the content.